Article type: Full Paper

Protein-sized Dye-loaded Polymer Nanoparticles for Free Particle Diffusion in Cytosol

Andreas Reisch, Doriane Heimburger, Pauline Ernst, Anne Runser, Pascal Didier, Denis Dujardin, and Andrey S. Klymchenko**

Dr. A. Reisch, D. Heimburger, P. Ernst, A. Runser, Prof. P. Didier, Dr. D. Dujardin, and Dr. A. S. Klymchenko

Laboratoire de Bioimagerie et Pathologies, UMR 7021 CNRS, Faculté de Pharmacie, Université de Strasbourg, 67401, Illkirch, France.

E-mail: reisch@unistra.fr, andrey.klymchenko@unistra.fr

Keywords: fluorescent polymer nanoparticles, single-particle tracking, intracellular particle sieving, diffusion in the cytosol

Abstract:

How small should nanoparticles be in order to travel freely through the cytosol similar to proteins? Answering this question remains a challenge, because the majority of nanoparticles are relatively large and their size cannot be finely tuned to match that of proteins. Here, we develop poly(methyl methacrylate) copolymers with varied fraction and type of charged groups (carboxylate, sulfonate, trimethylammonium), yielding nanoparticles with controlled sizes from 50 to 7nm through nanoprecipitation. Loading these nanoparticles with a rhodamine dye/bulky counterion pair at 10wt% makes them highly fluorescent. After their coating with PEG-groups for preventing non-specific protein binding, they were microinjected into living cells, which enabled the first systematic study of the size-effect on diffusion in the cytosol for solid nanoparticles of the same nature. Single-particle-tracking data provides evidence for distinct particle-sieving in the cytosol in the size range from <10 to 50nm, suggesting that only nanoparticles smaller than a critical size of 23nm exhibit free diffusion and spreading. These findings show the size limitations imposed by intracellular crowding and compartmentalization, which is critical for applications of nanomaterials in the cytosol. The proposed concept of polymer-design opens the route to organic nanoparticles of ultrasmall sizes and high loading for bioimaging and drug-delivery applications.

1. Introduction

Proteins are nature's ultimate nanoparticles (NPs), combining a large spectrum of functionalities with highest specificity, a size small enough to access nearly any desired location, and biodegradability. In consequence, ultrasmall polymer NPs mimicking their behavior have a high potential as bioimaging agents and drug carriers.[1,2] They could, for example, play a key role in single-molecule imaging of biomolecules inside living cells using fluorescence microscopy. Studying the behavior of single molecules is of key importance for the understanding of biological processes at the molecular level, but requires labelling of the biomolecules of interest with fluorescent probes.[3–5]. The speed and resolution, with which the biomolecules can then be tracked, depend on the number of collected photons.[6] In consequence, the brightness of the probe is particularly important, especially as already quite low light intensities can alter the behavior of cells.[7–9] At the same time the probes themselves should not interfere with the studied biological systems. Ideal probes would thus combine high brightness with small size, close to that of single proteins,[10,11] and absence of non-specific interactions.[12–14]

The limited brightness of organic fluorophores and fluorescent proteins, such as GFP, can be overcome by using fluorescent nanoparticles (NPs).[15–17] The most popular examples include quantum dots,[13,18–20] dye-doped silica NPs,[21] NPs based on the assembly of dyes,[22,23] conjugated polymer NPs,[24–27] aggregation induced emission NPs,[28,29] dye-loaded polymer NPs,[30,31] etc. The latter appeared recently as systems with exceptional brightness,[32,33] which already found applications in super-resolution imaging,[32] amplified single-molecule detection,[34] and multicolor cellular imaging.[35,36]

Non-specific interactions of nanoparticles with biological molecules, on the other hand can be suppressed through modification of the surface with polyethylene glycol (PEG) or other hydrophilic groups as zwitterions.[37,38] However, what is the ideal size of NPs for intracellular applications, notably in view of the crowded and complex structure of the cytosol?[39–44] Do NPs have to be as small as proteins, or is the size of endosomes sufficient? Indeed, while the influence of NP size on their fate *in vivo*[45,46] or on the interactions with cells has been evaluated in detail,[47,48] studies on its influence on intracellular diffusion of solid NPs, especially on the single particle level, are largely missing. Size dependence of intracellular behavior has, up to now, mainly been studied for macromolecules as dextrans[49] and DNA[50] using ensemble methods.[41,42,51] These macromolecular nanoscale objects are, however, expected to behave, in view of their deformability, totally different from "hard" (solid) NPs, such as quantum dots, magnetic, carbon and silica nanoparticles or NPs based on hydrophobic

polymers. Although the solid particles has been extensively studied in biological and biomedical fields for imaging to drug delivery applications,[15,16,52–54] the effect of their size on the intracellular diffusion at single-particle level has not been systematically investigated. A probable reason is that it remains a challenge to prepare a series of fluorescent NPs of the same nature with finely tuned sizes down to the level of single proteins, while maintaining a sufficient brightness for single-particle visualization.[55] To evaluate the optimal size for intracellular imaging we consider dye-loaded polymer NPs to be excellent candidates.

Approaches to the synthesis of small polymeric NPs include notably different types of emulsion polymerizations[56,57] and self-assembly of block copolymers.[58,59] Nanoprecipitation of preformed polymers is a simple technique for preparation of NPs, which also allows encapsulation of drugs and contrast-agents.[60,61] In order to reduce the size of polymeric NPs in the latter case, controlling the parameters of nanoprecipitation, e.g. the presence of charged groups,[62] concentration,[63] mixing speed,[64] and type of solvent,[65] can be successfully employed. However, so far, dye-loaded polymer NPs, assembled through nanoprecipitation, had never reached sizes of ≤10 nm, which would match dimensions of proteins. Here, we varied the type and the fraction of charged groups on poly(methyl methacrylate) (PMMA) to reduce maximally the size of dye-loaded polymer NPs. This allowed us to create series of particles of the same nature and surfaces but varying size. We then studied the influence of the size and surface of these particles on their behavior in the cytosol. The observed size-dependent diffusion of the particles has profound consequences for understanding steric restrictions imposed by the cytosol on nanomaterials, which is of key importance for their intracellular applications.

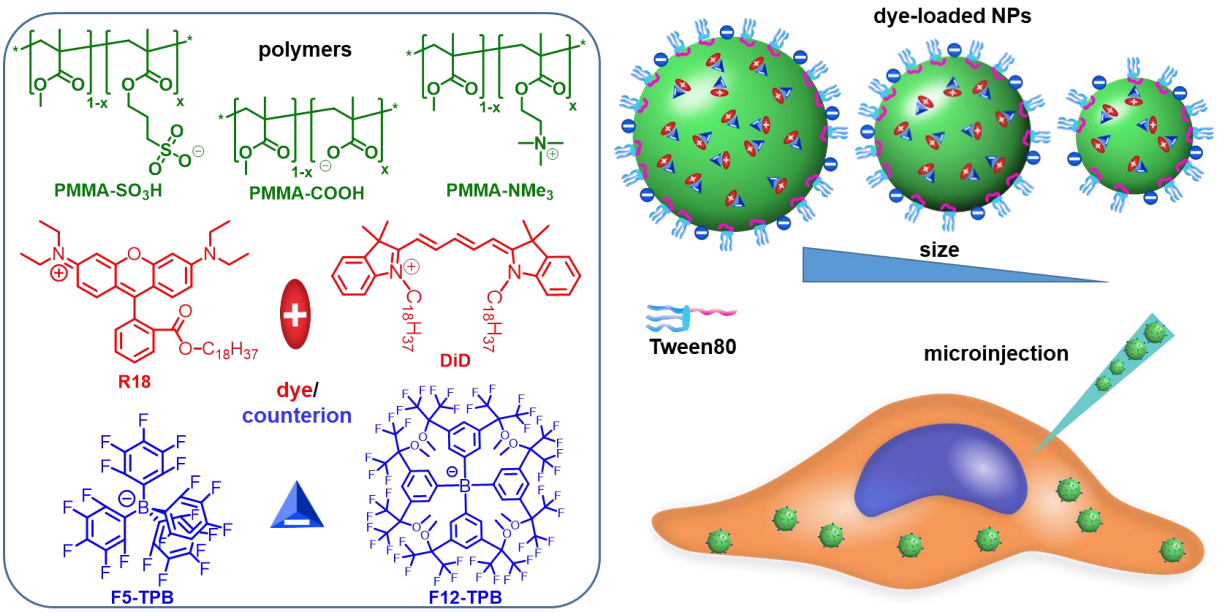

Scheme 1. Structures of polymers, dyes, and counterions used in this study, and schematic representation of preparation of dye-loaded nanoparticles of different sizes and their microinjection.

2. Results and Discussion

2.1. Polymer Synthesis and Nanoparticle Assembly and Characterization

Three series of methyl methacrylate based copolymers bearing either carboxylic acid, sulfonate or trimethylammonium groups in their side chains were synthesized (Scheme 1). The percentage of charged groups was varied from 1 to 10 mol%. Polymerization yielded copolymers with molecular weights around 50,000 for carboxylate and sulfonate polymers and 90,000 for trimethylammonium polymers. The fraction of charged groups in the polymers could be well controlled and was, according to NMR, close to the fraction in the feed. These polymers dissolved in acetonitrile were then nanoprecipitated in water to yield NPs. Their size decreased systematically with increasing percentage of charged groups (Figure 1). For sulfonate and trimethylammonium bearing polymers the size reached 8 and 7 nm, respectively, at ≥5% of charged groups. This corresponds to approximately 8 and 4 polymer chains per NP at the obtained molecular weights. At 10% of sulfonate groups transmission electron microscopy (TEM) images did not show particles anymore, but rather deposition of unstructured polymer, indicating a limit to particle formation. Particles made from carboxylate bearing polymers were systematically larger, though the size was reduced using buffer at pH 7.4 (Figure S2). Fluorescence correlation spectroscopy (FCS) was used to measure the hydrodynamic diameter of the particles (Figure 2). These results confirmed the

trends observed by TEM, giving nearly identical sizes for the small sulfonate particles (17, 13, and 9 nm for 1, 2, and 5% PMMA-SO_3H NPs, respectively), and a bit larger sizes for the larger NPs (86 nm for PMMA-COOH 1% NPs and 53 nm for PMMA-SO_3H 1% NPs made in 30 mM NaCl) due to the stronger contribution of larger particles to the fluorescence signal.

For sulfonate and trimethylammonium polymers the number of charged groups per particle was around 100 independently of polymer composition and thus particle size (Table S1). Particle growth and thus incorporation of new polymers in the NPs, hence, stopped once this threshold was reached, probably due to electrostatic repulsion. In consequence the particle size decreased for more charged polymer. In MilliQ water the Debye screening length exceeds 10 nm and thus all the charges on these small NPs can contribute to repulsion of an incoming chain. By contrast, the effective charge of the carboxylate groups in MilliQ water is lower, and the particles thus reach sizes lager than the Debye screening length. In consequence, particle growth is stopped only when a given surface charge density is reached, as observed previously.[66,67] Importantly, addition of NaCl in the precipitation medium that decreases these repulsive forces allowed us to increase the size of particles made from a given polymer (Figure 1).

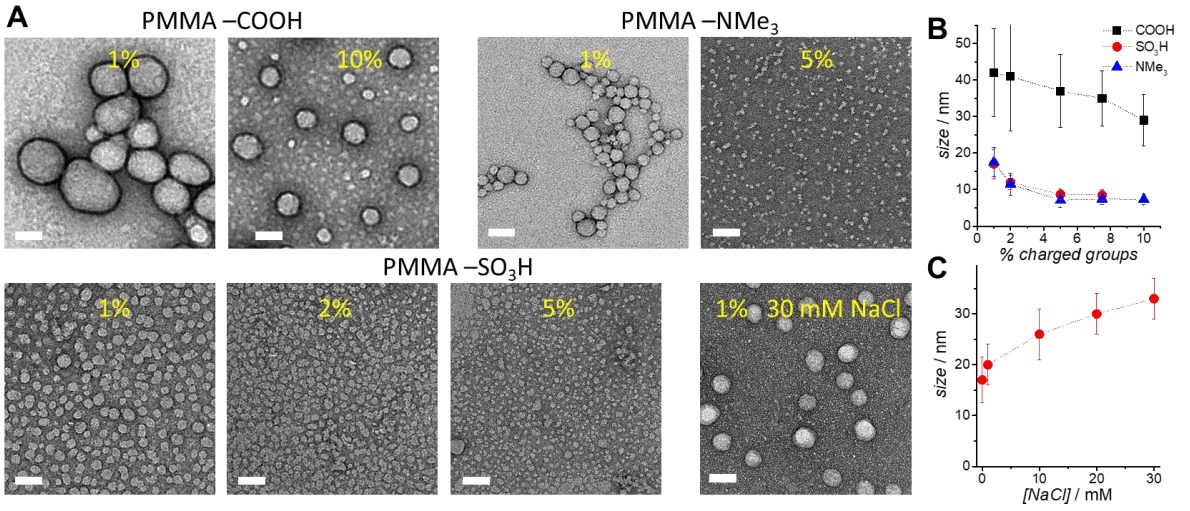

Figure 1. Sizes of NPs made by nanoprecipitation: (A) TEM images of NPs made from different polymers in water or 30 mM NaCl. Scale bars, 50 nm. (B) Influence of the fraction of charged groups on the size of NPs. (C) Influence of NaCl concentration in the precipitation medium on the size of PMMA-SO_3H 1 % NPs. In (B) and (C), mean values of sizes determined by TEM are given for NPs loaded with 10 wt% of R18/F5-TPB. At least 200 NPs were analysed per condition. Error bars give full width at half maximum of the distribution.

These NPs were made fluorescent through the encapsulation of 10 wt% of a rhodamine dye salt (R18/F5-TPB, wt% relative to polymer, Scheme 1).[32] The bulky counterion prevents aggregation of dyes in the polymer matrix, leading to high fluorescence quantum yields ~50 % even at this high loading (Table S2). Consequently, the estimated brightness of 17, 12 and 9 nm PMMA-SO3H NPs was 7 x 10^6, 2 x 10^6 and 7 x 10^5 M cm-1, respectively, that is 25, 10, and 3 times higher than that of corresponding quantum dots (QD585) at 532 nm excitation. Fluorescence microscopy of single particles immobilized on surfaces confirmed these estimations (Figure 3 A and Figure S4), showing that our NPs are brighter than QDs despite their much smaller size.

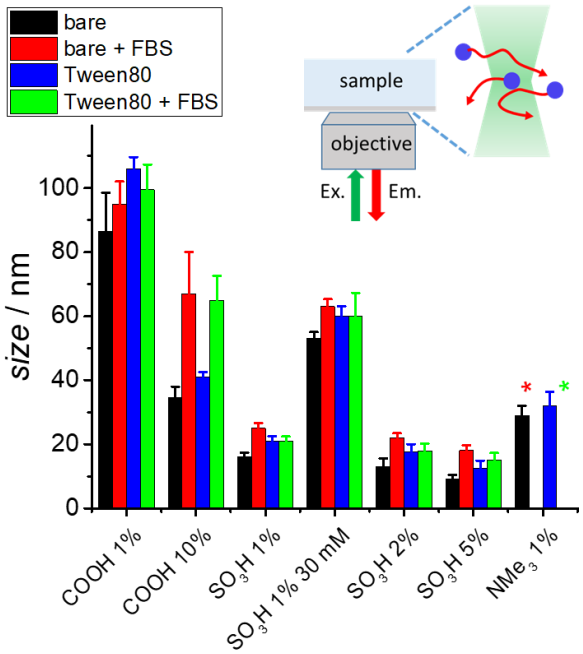

Figure 2. Fluorescence correlation spectroscopy (FCS) on dye-loaded polymer NPs: Hydrodynamic sizes of NPs with and without surface treatment with Tween80 in differet conditions as determined by FCS. Given are the sizes of as made NPs, NPs exposed to 10 vol% FBS solution, NPs pre-treated with 0.05 mg/mL Tween80 and then exposed or not to 10 vol% FBS solution. NPs were loaded with 1 or 2 wt% of R18/F5-TPB. Error bars give SEM over 3 measurements. *Aggregation or no particles were detected. Inset: Schematic view of the FCS technique.

2.2. Microinjection of Nanoparticles

In order to render these NPs resistant to protein adsorption they were treated with Tween80, a PEG bearing surfactant.[62] Their interaction with serum proteins was then studied with fluorescence correlation spectroscopy (FCS, Figure 2). Adsorption of Tween80 led to an increase of the particle size by ~5 nm, which suggests adsorption of a monolayer. When solutions of 10% fetal bovine serum (FBS) were added to the resulting particles, the particle size for PMMA-SO_3H and 1%-PMMA-COOH NPs did not change, suggesting that a monolayer of Tween80 is sufficient to suppress non-specific interactions with serum proteins. The behavior of these NPs treated with Tween80 and having different sizes was then studied in the cytosol. For this we microinjected solutions of NPs directly into the cytosol of living HeLa cells (Figure 3 B, Figure S5 for other NP types, videos in SI). Dye leaching from all used nanoparticles was virtually absent, at least on the time scale of our study. Indeed, no diffuse intracellular labeling (notably of mitochondria) was observed, as would be expected for the case of leaching of the used R18 dye.[68,69] Individual nanoparticles and their movement could be easily observed and tracked inside cells at low illumination intensities (2 $W.cm^{-2}$). The vast majority of larger NPs (42 nm, and 29 nm NPs made of PMMA-COOH 1% and 10%, respectively, and 32 nm PMMA-SO_3H 1% particles, made in 30 mM NaCl) remained close to the point of injection. Only very few of these particles actually moved inside the cell and their movements were restricted to the immediate surroundings of the injection point. However, smaller NPs of 17 nm, made from PMMA-SO_3H 1% in MilliQ water, spread practically through the entire cell. Most (~90%) of these particles moved quickly throughout the cytosol (Figure 2C, left and middle). This suggests a critical size required for efficient spreading throughout the cytosol. A closer look at the image sequences shows that some particles from 32-nm formulation spread inside the cells, whereas about 10 % of particles from 17-nm formulation remained close to the point of injection. This phenomenon can be explained by non-negligible size distribution in these two formulations of NPs. The particle size distribution of the NPs from the 17-nm formulation (insets in Figure 3B) shows that about 10 % of the particles are larger than 23 nm, while about 5% of NPs from the 32-nm formulation are smaller than 23 nm. This indicates that the actual critical size of the hard particle core for spreading throughout the cytosol is situated at around 23 nm.

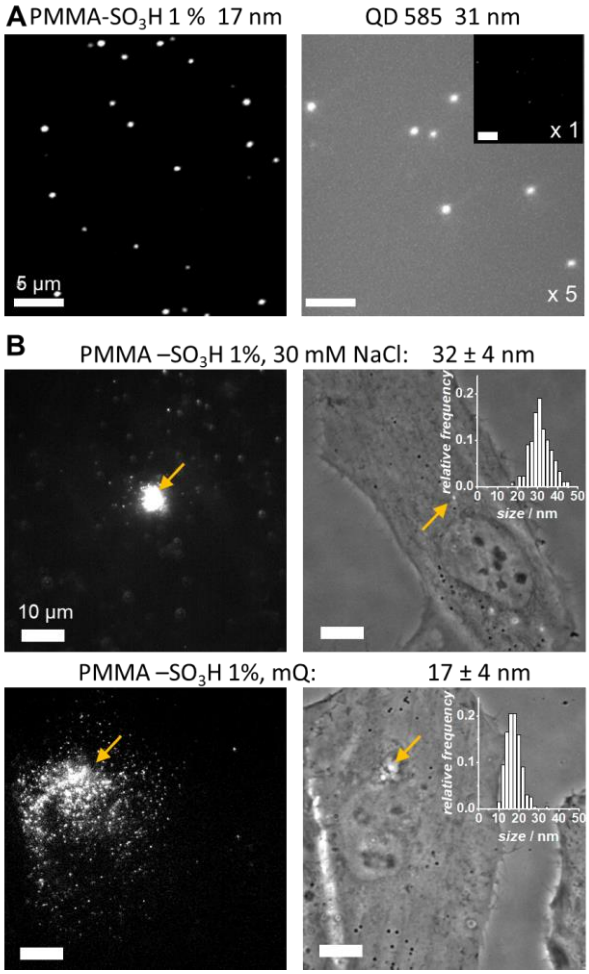

Figure 3. Microscopy of NPs on surfaces and in the cytosol. (A) Microscopy images of PMMA-SO_3H 1% NPs loaded with 10 wt% R18/F5-TPB and of QDs 585 immobilized on a surface in TIRF mode (532 nm laser excitation, 12 W/cm^2). For better visibility the QD intensity was increased fivefold (original in inset). Scale bars, 5 µm. (B) Microinjection of NPs in living HeLa cells. Left-hand: epi-fluorescence micrographs of 32 and 17 nm PMMA-SO_3H 1% NPs made in 30 mM NaCl and MilliQ water, respectively. Right-hand: phase-contrast images of the corresponding cells. Injection points are indicated by arrows. Scale bars, 10 µm. Insets show distributions of particle sizes obtained by TEM. NPs were loaded with 10 wt% of R18/F5-TPB and coated with Tween 80.

We then studied the intracellular movement of these NPs in more detail. In particular, we wanted to know, whether and how a further reduction in the size of NPs would influence their movement inside cells. PMMA-SO_3H NPs of 12 and 9 nm size, as those of 17 nm, spread well throughout the cells and retained a high mobility (Figure 4 and SI Figure S5). A particularly good impression of the spreading of the particles can notably be obtained through a maximum projection of the particle fluorescence over a given observation time (Figure 4 A

and Figure 5). We then performed single particle tracking analysis on 17 nm and 9 nm particles using threefold lower particle concentration and a microscope operating in highly inclined and laminated optical sheet (HILO) mode[70] with laser illumination and an EMCCD camera. Plotting mean square displacement (MSD) versus time for individual trajectories allows characterizing the diffusion behavior, such as diffusion coefficient and type of diffusion (i.e. free, restricted diffusion or their combination, Figure 4 B).[42,71,72] First, the initial slope can be used to extract the diffusion coefficient on a local scale for the two-dimensional projection.[71,72] Both 17 and 9 nm NPs showed a broad (nearly bimodal) distribution of diffusion times, indicating that the diffusion of part of NPs (about 30%) was significantly slowed, probably due to non-specific interactions or a strong spatial restriction (Figure 4 B, C1, D1). The diffusion coefficients were centered ~0.7 µm²/s for the 17 nm NPs and ~1.5 µm²/s for the 9 nm NPs, corresponding to the higher mobility of the smaller particles. These values are considarably higher than diffusion coefficients obtained for quantum dots in the cytosol,[73–75] in line with the smaller size of our NPs. Second, further information on the movement of the particles can be obtained from the shape of the plots of MSD as a function of lag time (Figure 4 C2, C3, D2, D3): Free Brownian diffusion is seen as a straight line; occurrence of plateaus or kinks indicates confined (restricted) diffusion, with the position of the plateau giving access to the size of the involved structures; and upward bending of the curves indicates superdiffusion often due to an active transport or a flow.[42,71,72] The latter was virtually absent for both particle sizes analyzed here. The relative importance of free-diffusive and subdiffusive behavior, however, was significantly different for 17 vs 9 nm NPs. In the case of 9 nm NPs more than 60 % of the MSD curves were entirely straight indicating free diffusion. These corresponded mainly to those having high initial diffusion coefficients. Interestingly from the curves having visual kinks, corresponding to restrited diffusion, about 75% showed a stabilization or even a regain in the slope of the curve after the kink (Figure 4 C bottom right). This behavior indicates that the particles were able to overcome the spatial restrictions.[42,72] In the case of the 17 nm NPs only about 40 % of the particles showed relatively straight MSD curves corresponding to free Brownian diffusion. Furthermore, in the cases where the MSD curves showed kinks, most actually reached plateau values, indicating that particle movement was indeed restricted to certain regions.

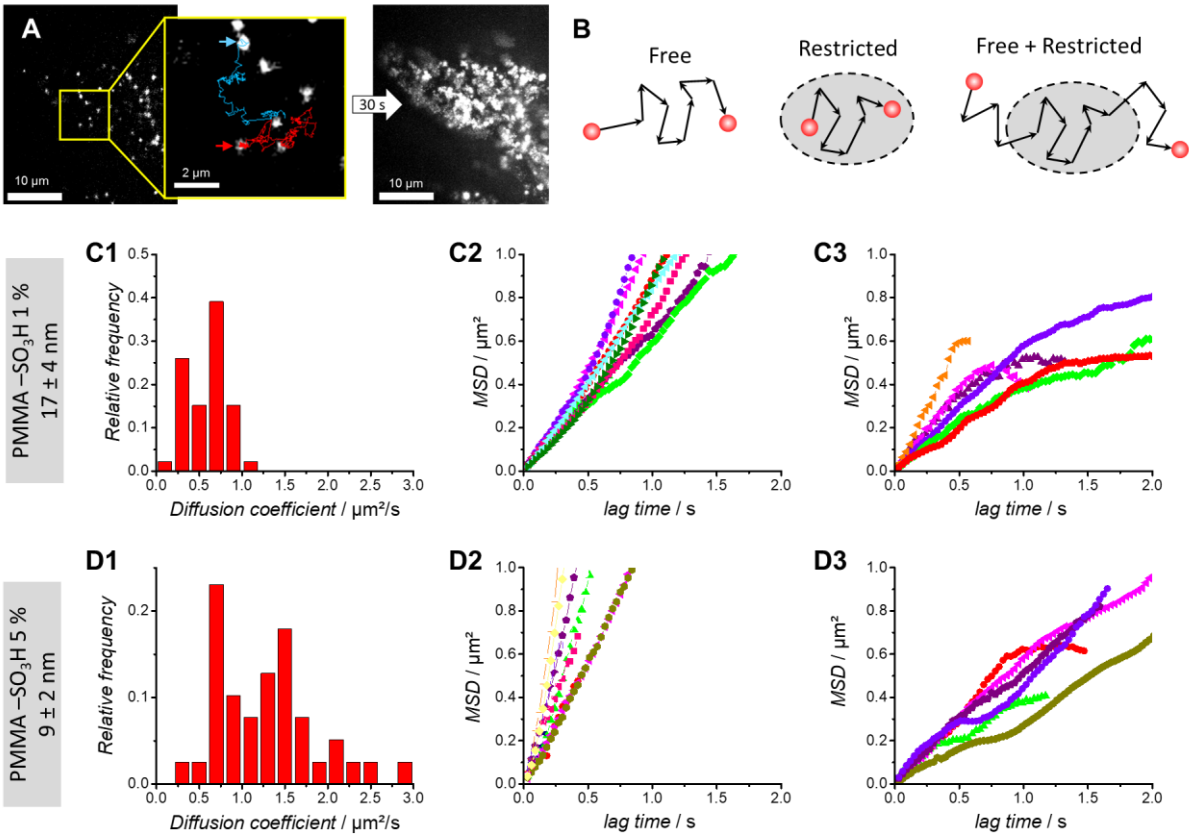

Figure 4. Diffusion of nanoparticles in the cytosol studied by single-particle fluorescencce microscopy. (A) 17 nm PMMA-SO_3H NPs in a HeLa cell (HiLo mode, 532 nm laser excitation, 2 W/cm², 30 ms per frame). The trajectories of two particles (arrows) are shown. Right-hand: maximum projection of the acquisition over 30 s. NPs were loaded with 10 wt% of R18/F5-TPB and coated with Tween 80. (B) Three simplified cases of intracellular diffusion: free, restricted and combination of free and restricted diffusion. Analysis of single particle trajectories for PMMA-SO_3H 1% 17 nm NPs (C1-C3) and PMMA-SO_3H 5% 9 nm NPs (D1-D3). (C1, D1) Distribution of diffusion coefficients as obtained from the initial slope of the MSD curves. (C2, C3, D2, D3) MSD vs lag time for several representative trajectories, showing straight curves (C2, D2) and kinks (C3, D3). At least 60 trajectories from 3 different cells were analyzed per condition.

In order to directly compare the intracellular behavior of different NPs of close sizes, (and thus overcome cell-to-cell variations in injection or morphology), we performed pairwise comparison of a subset of NPs co-injected in the same cell. For this, we labelled two different types of NPs to be compared with dyes of different colors, a rhodamine (R18/F5-TPB) and a cyanine 5 (Cy5/F12-TPB) (Scheme 1), mixed them at equivalent particle concentrations, and injected them together, before imaging them in two separate channels (Figure 5). Comparison

of the 32 and 17 nm PMMA-SO_3H NPs confirmed the differences observed when injecting the particles in different cells (Figure 5 A and Figure 3 B): localization and immobilization of the larger NPs around the injection point and spreading of the smaller ones. Co-injecting 17 and 12 nm PMMA-SO_3H NPs showed that both spread through the entire cell (Figure 5 B). However, the 17 nm NPs were excluded from several intracellular regions where the 12 nm NPs had access (lower panels in Figure 5 B). Finally, a comparison of 12 and 9 nm PMMA-SO_3H NPs showed slightly better accessibility of the latter mainly at the edge of cells with a flat morphology (Figure 5 C).

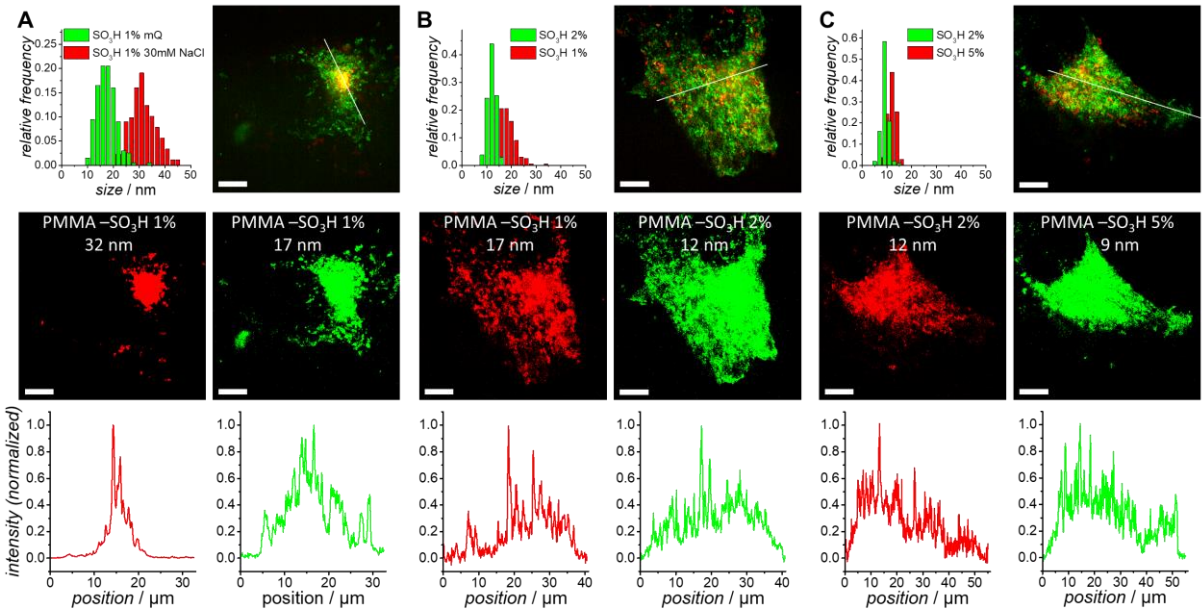

Figure 5. Two-color imaging of different sets of PMMA-SO_3H NPs co-microinjected into the cytosol. (A) 32 nm (red) and 17 nm (green) NPs, prepared from PMMA-SO_3H 1% in 30 mM NaCl and MilliQ water, respectively. (B) 17 nm (red) and 12 nm (green) NPs. (C) 12 nm (red) and 9 nm (green) NPs. Particles presented in red were loaded with 20 mM Cy5/F12-TPB, particles in green with 10 wt% of R18/F5-TPB, all were coated with Tween 80. In each part the panels represent: top left: size distributions from TEM; top right: superposition of maximum projections over 1 min; middle: threshold images obtained from the projections; bottom: intensity profiles along the lines indicated in top right. Scale bars, 10 µm.

We thus observed distinct diffusion behavior of solid nanoparticles depending on their size: Particles with sizes of 32 nm remained (on the time scale of our experiments) confined to the region of injection. Particles of 17 nm already spread throughout the entire cell. Comparison of the size distributions for these two types of NPs gave a critical size of 23 nm, below which NPs tended to spred well inside the cells. Smaller NPs of 12 and 9 nm showed improved

access to some regions of the cytosol. Especially the 9 nm NPs were capable to access regions at the edge of the cell, and were, based on the MSD curves better capable to escape from restricted compartments. It should be taken into account that the particle sized described here correspond to hard-sphere diameters estimated from TEM, whereas intracellular diffusion should be governed by the hydrodynamic diameter, which is somewhat larger (Figure 2).

These results can be compared to previous experimental data using mostly ensemble methods and deformable macromolecules as well as to different approaches to model diffusion in the cytosol.[39,40,42,51,76] From a structural point of view a major barrier to diffusion is the cytoskeleton. Using different methods, mesh sizes in the range of 30 to 100 nm were found,[77,78] although even smaller particles of 10 nm were restricted in their movement by the actin cytoskeleton.[79] A second barrier to diffusion, notably in the perinuclear region, is constituted by the endoplasmatic reticulum (ER) and the Golgi apparatus. It has notably been observed that QDs of 27 nm and macromolecules of 48 nm were restricted in their movement by the ER and the trans-Golgi.[73,77] The increased density and finely divided filaments of the cytoskeleton at the edge of the cells were noted to restrict the access of macromolecules further, leading to strongly decreased partitioning for macromolecules larger than 20 nm.[77,80] The nucleus finally was only accessible to macromolecules smaller than 7 nm.[49] This suggests that spreading of our larger particles, injected in the perinuclear region, is limited by the ER and the Golgi in combination with the cytoskeleton. The critical size of 23 nm revealed in our work for hard particles is in good agreement with the lower mesh sizes found for the cytoskeleton (30 nm). This suggests that the smallest mesh sizes are effective for restricting the motion of hard particles. The diffusion restrictions for intermediate sized particles of 17 nm, could notably stem from the spaces in-between cisternae of the Golgi and in voids of the ER, which create small compartments. Smaller particles can probably still escape relatively quickly from such compartments. Our results showed that particles larger than 10 nm were at least partially excluded from the edges of the cells, indicating again that the critical sizes for hard particles are smaller than those for deformable macromolecules. Finally, our particles did not significantly enter the nucleus and did not appear to localize specifically inside other intracellular compartments, in line with the size restrictions mentioned above.

In a different approach, the so-called length-scale dependent viscosity model, the cytosol is considered as a heterogeneous, crowded mixture and the viscosity experienced by a probe depends on its size (relative to that of the crowding agent) and on the relative crowding.[42,51] Two limiting dimensions of the diffusing particles emerge from this model: Particles smaller

than the correlation length feel the nanoscale viscosity of the solution and basically move freely in-between the obstacles. Particles with sizes above the limiting length, on the other hand, are subject to the macroscale viscosity. For these particles the cytosol resembles a gel or even a colloidal glass strongly restricting their motion. For HeLa and Swiss 3T3 cells these lengths were found, mainly based on DNA and dextrans, to be respectively 5 and 7 nm for the correlation length and 86 and 30 nm for the limiting size. Similar results were found for bacterial cytoplasm, with a critical size in the range of 30-40 nm for the diffusion of protein based particles. Above this size the bacterial cytoplasm showed glass-like properties in the absence of metabolic activity.[81] With respect to this model even the sizes of the smallest particles studied here were already above the correlation length. The critical size of 23 nm found here is of the same order, yet again below that found for deformable macromolecules. Together these results show the influence and importance of particle size for the behavior of solid NPs, and, how these differ from the results obtained for deformable macromolecules, even though they follow the same trends.

3. Conclusions

In order to address the question of the optimal size of nanoparticles for intracellular applications, we designed a series of dye-loaded polymer NPs with finely tuned sizes. The control of the fraction of charged groups, notably sulfonate and trimethylammonium, allowed achieving particle sizes below 10 nm, and thus attaining the sizes of proteins. Despite their small size these particles could be made brightly fluorescent (3-25 fold brighter than corresponding quantum dots) by encapsulating dyes at high concentration. This in turn made them suitable for single-particle tracking inside the cytosol even at low light excitation intensities. Using a series of NPs with sizes of 9, 12, 17 and 32 nm, we could evaluate for the first time the influence of particle size on the movement of solid particles in the cytosol: NPs below a critical size of ≤23 nm were required to obtain spreading throughout the living cell. Still smaller particle sizes are required to quickly reach all regions of the cytosol. Our findings on the size-dependent intracellular diffusion of solid particles are of highest importance for practically any application of nanoparticles in the complex intracellular environment. Moreover, our concept of polymer design opens the route to organic nanoparticles of ultrasmall sizes, which should enable high-speed tracking of single biomolecules with high localization precision.

4. Experimental Section

Materials: Methyl methacrylate (99 %), methacrylic acid (99 %), 3-sulfopropyl methacrylate potassium salt (98 %), [2-(methacryloyloxy)ethyl]trimethylammonium chloride (75 % in water), acetonitrile (anhydrous, 99.8%), rhodamine B octadecyl ester perchlorate (>98.0%), lithium tetrakis(pentafluorophenyl)borate ethyl etherate were purchased from Sigma-Aldrich. R18/F5-TPB, the salt of Rhodamine B octadecyl ester with tetrakis(pentafluorophenyl)borate, and Cy5/F12-TPB, the salt of DiD with sodium tetrakis[3,5-bis(1,1,1,3,3,3-hexafluoro-2-methoxy-2-propyl)phenyl]borate trihydrate were synthesized through dye exchange followed by purification through column chromatography as described previously.[32,35] MilliQ-water (Millipore) was used in all experiments. Qdot® 585 Streptavidin Conjugates were purchased from Thermo-Fisher Scientific.

Synthesis of polymers: The different polymers were synthesized through free radical polymerization. Methyl methacrylate and the corresponding charged monomer were both dissolved in degased acetonitrile or DMSO and mixed at the desired ratio. 0.01 eq. of AIBN were added and the round bottom flask was placed in an oil bath preheated to 70 °C. Once the conversion reached 25 %, the reaction was stopped and the polymers reprecipitated twice in methanol and/or water. After drying, the polymers were characterized through NMR and size exclusion chromatography.

Poly(methyl methacrylate-co-methacrylic acid) (PMMA-COOH): Methyl methacrylate and methacrylic acid were both dissolved in degased acetonitrile at a concentration of 1 M. The two solutions were then mixed in a 100 mL two-neck round bottom flask equipped with a stirring bar at the desired ratio to give a total volume of 40 mL (e.g. for 1 % of methacrylic acid: 39.6 mL of methyl methacrylate solution and 0.4 mL of methacrylic acid solution). The mixture was degazed by bubbling argon for 5 min and placed under argon atmosphere. 0.01 eq of AIBN in acetonitrile (40 mg/mL) were added and the round bottom flask was placed in an oil bath preheated to 70 °C. At regular intervals samples were drawn, dissolved in DMSO-d_6 and analyzed by NMR. Once the conversion reached 25 %, the reaction was stopped by quickly cooling it to RT. Part of the acetonitrile was evaporated under reduced pressure and the reaction mixture was added dropwise to methanol. After filtration the precipitate was redissolved in a small amount of acetonitrile and reprecipitated twice in methanol. The obtained polymer was dried under vacuum. ^{1}H NMR (400 MHz, $CDCl_3$, δ): 3.60 (s, 3 H), 2.2 – 0.5 (m, 6 H). Molecular weight by GPC: 1%: M_w = 38 100, M_w /M_n = 1.35; 5%: M_w = 46 800, M_w /M_n = 1.34.

Poly(methyl methacrylate-co-3-sulfopropyl methacrylate) (PMMA-SO_3H): Methyl methacrylate and 3-sulfopropyl methacrylate potassium salt were dissolved in degased DMSO at a concentration of 2 M. The two solutions were then mixed in a 50 mL two-neck round bottom flask equipped with a stirring bar at the desired ratio to give a total volume of 20 mL. The mixture was degased by bubbling argon for 5 min and placed under argon atmosphere. 0.01 eq. of AIBN in DMSO (40 mg/mL) were added and the round bottom flask was placed in an oil bath preheated to 70 °C. At regular intervals samples were drawn, dissolved in DMSO-d_6 and analyzed by NMR. Once the conversion reached 25 %, the reaction was stopped by quickly cooling it to RT. The reaction mixture was then added dropwise to methanol, or, for higher percentages of the charged monomer, to water. After filtration, the precipitate was redissolved in a small amount of acetonitrile and reprecipitated twice in methanol (water for highest percentages). The obtained polymer was dried under vacuum. ^{1}H NMR (400 MHz, DMSO-d_6, δ): 3.97 (br. s, 0.02-0.2 H), 3.57 (s, 3 H), 2.45 (m, partial covered by the solvent peak), 2.1 – 0.5 (m, 6 H). Fraction of SO_3H groups based on the peak at 3.97 ppm (feed: obtained): 1%: 1.1%; 2%: 2.3%; 5%: 5.5%, 10%: 12%. Molecular weight by GPC: 1%: M_w = 51 200, M_w /M_n = 1.58; 5%: M_w = 48 400, M_w /M_n = 1.08.

Poly(methyl methacrylate-co-[2-(methacryloyloxy)ethyl]trimethylammonium) (PMMA-NMe_3): Methyl methacrylate was dissolved in degased DMSO at a concentration of 2 M. [2-(methacryloyloxy)ethyl]trimethylammonium chloride was diluted with DMSO to yield a 2 M solution. The two solutions were then mixed in a 50 mL two-neck round bottom flask equipped with a stirring bar at the desired ratio to give a total volume of 20 mL. The mixture was degased by bubbling argon for 5 min and placed under argon atmosphere. 0.01 eq. of AIBN in DMSO (40 mg/mL) were added and the round bottom flask was placed in an oil bath preheated to 70 °C. At regular intervals samples were drawn, dissolved in DMSO-d_6 and analyzed by NMR. Once the conversion reached 25 %, the reaction was stopped by quickly cooling it to RT. The reaction mixture was then added dropwise to methanol, or, for higher percentages of the charged monomer, to water. After filtration, the precipitate was redissolved in a small amount of acetonitrile and reprecipitated twice in methanol (water for highest percentages). The obtained polymer was dried under vacuum. ^{1}H NMR (400 MHz, DMSO-d_6, δ): 4.37 (br. s, 0.02-0.2 H), 3.70 (br. S, 0.02-0.2), 3.55 (s, 3 H), 3.17 (s, 0.09 – 0.9 H), 2.1 – 0.4 (m, 6 H). Fraction of NMe_3 groups based on the peak at 3.17 ppm (feed: obtained): 1%: 1.1%; 2%: 2.4%; 5%: 5.8%, 10%: 12.2%.Molecular weight by GPC: 1%: M_w = 99 900, M_w /M_n = 1.62; 5%: M_w = 95 300, M_w /M_n = 1.22.

Preparation of NPs: Solutions of the polymers at 2 mg mL^{-1} in acetonitrile (up to 15 vo.l% methanol for >5% charged groups), containing the desired amount of dye (1, 10 or 20 wt% relative to the polymer) were added quickly and under stirring (shaking) using a micropipette to a 10-fold volume excess of water, NaCl solution, or 20 mM pH 7.4 phosphate buffer at 21 °C. The particle solution was then quickly diluted five-fold in water.

For FCS experiments these solutions were diluted twofold, and Tween80 was added to obtain a Tween80 concentration of 0.05 g/L. For cell experiments the particle solutions were diluted to a particle concentration of 2 to 5 nM, followed by the addition of Tween80 to obtain a Tween 80 concentration of 0.05 g/L.

Characterization of NPs:

Absorption and emission spectra were recorded on a Cary 4000 Scan ultraviolet–visible spectrophotometer (Varian) and FluoroMax-4 spectrofluorometer (Horiba Jobin Yvon) equipped with a thermostated cell compartment, respectively. QYs were calculated using rhodamine 101 in ethanol as standard (QY = 0.9).[82]

Electron Microscopy: 5 µL of the particle solution were deposited onto carbon-coated copper-rhodium electron microscopy grids that were used either as obtained or following an air or amylamine glow-discharge. The grids were then treated for 1 min with a 2 % uranyl acetate solution for staining and observed with a Philips CM120 transmission electron microscope equipped with a LaB_6 filament and operating at 100 kV. Areas covered with NPs of interest were recorded at different magnifications on a Peltier cooled CCD camera (Model 794, Gatan, Pleasanton, CA). Image analysis was performed using the Fiji software.

Fluorescence Correlation Spectroscopy (FCS): FCS measurements were performed on a home-built confocal set-up based on a Nikon inverted microscope with a Nikon 60x 1.2NA water immersion objective. Excitation was provided by a cw laser diode (532 nm, Oxxius) and photons were detected with a fibered Avalanche Photodiode (APD SPCM-AQR-14-FC, Perkin Elmer) connected to an on-line hardware correlator (ALV7000-USB, ALV GmbH, Germany). Typical acquisition time was 5 min (10 × 30 s) with an excitation power of 0.5 mW at the sample level. The data were analyzed using the PyCorrFit software.[83]

Fluorescence Microscopy: Two set-ups were used for fluorescence microscopy: Microinjection itself and part of the cellular single particle imaging (notably the two-color imaging) were performed on a Leica DMIRE 2 microscope equipped with a control system of 37 °C, 5% CO2 (Life Imaging Services), a 100 × HCX PL APO CS (1.4 NA) objective using a Photometrics Prime sCMOS camera piloted by the Metamorph software, a Xenon-lamp and

Leica Y3 and Y5 filter cubes. Single particle measurements and part of the intracellular single particle tracking were performed in the TIRF (Total Internal Reflection Fluorescence) or HILO mode on a home-made wide-field setup based on an Olympus IX-71 microscope with an oil immersion objective (NA = 1.49, 100x). A DPPS (Cobolt) continuous wave (CW) laser emitting at 532 nm was used for excitation at 12 $W.cm^{-2}$ for immobilized single particles, and at 2 $W.cm^{-2}$ for cellular imaging. The fluorescence signal was recorded with an EMCCD (ImagEM Hamamatsu) using an exposure of 30.5 ms per image frame. For single particle fluorescence microscopy measurements the NPs were immobilized either on glass surfaces on which a polyethyleneimine (PEI) layer was initially adsorbed or in 15 wt% poly(vinyl alcohol), as described previously.[11,32] The surfaces were left in MilliQ-water during microscopy. Quantum dots were immobilized and imaged in the same way as the NPs. Single particle analysis was performed using the Fiji software as described previously.[32,33]

Cellular experiments:

HeLa cells were grown in Dulbecco's modified Eagle medium (DMEM, without phenolred, Gibco-Invitrogen), supplemented with 10% fetal bovine serum (FBS, Lonza), L-glutamine, and 1% antibiotic solution (penicillin-streptomycin, Gibco-Invitrogen) at 37° C in humidified atmosphere containing 5% CO_2. Cells were seeded onto a round microscope cover glasses (diameter 18 mm) deposited in 6 well plates at a density of 125×10^3 cells/well 24h before the microinjection.

Microinjection of NPs and cellular imaging:

For microinjection experiments, subconfluent HeLa cells plated on glass coverslips were mounted in a Ludin Chamber (Life Imaging Services, Basel, Switzerland). The cells were then placed on the Leica DMIRE 2 microscope and solutions of the different nanoparticles at particle concentrations of 0.5 to 2 nM were microinjected into the perinuclear region of the cells, using a Femtojet/InjectMan NI2 microinjector (Eppendorf). Images sequences were then acquired either on the same setup or with the Olympus set-up used for single particle imaging after transfer of the samples. Time-lapse movies were analyzed using the ImageJ (National Institutes of Health, USA) software with the Mosaic module for single particle tracking[84]. Obtained trajectories were checked for artefacts (e.g. wrong connections, which were rare). At least three cells with 60 trajectories per condition were analyzed.

Supporting Information

Supporting Information is available from the Wiley Online Library or from the author.

Acknowledgements

This work was supported by the European Research Council ERC Consolidator grant BrightSens 648528 and by the Agence National de Recherche JC/JC grant "Supertrack" ANR-16-CE09-0007. The authors thank C. Ruhlmann and C. Crucifix from the FRISBI platform (ANR-10-INBS-05) for help with electron microscopy, R. Vauchelles and the QUEST platform imaging facility for help with fluorescence microscopy, P. Didier for help in the installation of the FCS setup, and M. Legros and C. Foussat for size exclusion chromatography.

Doriane Heimburger and Pauline Ernst contributed equally to this work.

References

[1] C. Wong, T. Stylianopoulos, J. Cui, J. Martin, V. P. Chauhan, W. Jiang, Z. Popović, R. K. Jain, M. G. Bawendi, D. Fukumura, *Proc. Natl. Acad. Sci.* **2011**, *108*, 2426.
[2] Y. Tsvetkova, N. Beztsinna, M. Baues, D. Klein, A. Rix, S. K. Golombek, W. Al Rawashdeh, F. Gremse, M. Barz, K. Koynov, S. Banala, W. Lederle, T. Lammers, F. Kiessling, *Nano Lett.* **2017**, *17*, 4665.
[3] S. Shashkova, M. C. Leake, *Biosci. Rep.* **2017**, *37*, BSR20170031.
[4] A. Kusumi, T. A. Tsunoyama, K. M. Hirosawa, R. S. Kasai, T. K. Fujiwara, *Nat. Chem. Biol.* **2014**, *10*, 524.
[5] A. J. Nelson, S. T. Hess, *J. Microsc.* **2014**, *254*, 1.
[6] H. Deschout, F. C. Zanacchi, M. Mlodzianoski, A. Diaspro, J. Bewersdorf, S. T. Hess, K. Braeckmans, *Nat. Methods* **2014**, *11*, 253.
[7] R. Dixit, R. Cyr, *Plant J.* **2003**, *36*, 280.
[8] J. Icha, M. Weber, J. C. Waters, C. Norden, *BioEssays* **2017**, *39*, 1700003.
[9] P. P. Laissue, R. A. Alghamdi, P. Tomancak, E. G. Reynaud, H. Shroff, *Nat. Methods* **2017**, *14*, 657.
[10] P. Çakir, A. Cutivet, M. Resmini, B. T. S. Bui, K. Haupt, *Adv. Mater.* **2013**, *25*, 1048.
[11] I. Shulov, R. V. Rodik, Y. Arntz, A. Reisch, V. I. Kalchenko, A. S. Klymchenko, *Angew. Chem. Int. Ed.* **2016**, *55*, 15884.
[12] C. Veigel, C. F. Schmidt, *Nat. Rev. Mol. Cell Biol.* **2011**, *12*, 163.
[13] F. Pinaud, S. Clarke, A. Sittner, M. Dahan, *Nat. Methods* **2010**, *7*, 275.
[14] S. J. Sahl, S. W. Hell, S. Jakobs, *Nat. Rev. Mol. Cell Biol.* **2017**, *18*, 685.
[15] O. S. Wolfbeis, *Chem. Soc. Rev.* **2015**, *44*, 4743.
[16] P. D. Howes, R. Chandrawati, M. M. Stevens, *Science* **2014**, *346*, 1247390.
[17] M. Elsabahy, G. S. Heo, S.-M. Lim, G. Sun, K. L. Wooley, *Chem. Rev.* **2015**, *115*, 10967.
[18] P. Pierobon, G. Cappello, *Adv. Drug Deliv. Rev.* **2012**, *64*, 167.
[19] L. Cognet, C. Leduc, B. Lounis, *Curr. Opin. Chem. Biol.* **2014**, *20*, 78.

[20] X. Michalet, F. F. Pinaud, L. A. Bentolila, J. M. Tsay, S. Doose, J. J. Li, G. Sundaresan, A. M. Wu, S. S. Gambhir, S. Weiss, *Science* **2005**, *307*, 538.
[21] S. Bonacchi, D. Genovese, R. Juris, M. Montalti, L. Prodi, E. Rampazzo, N. Zaccheroni, *Angew. Chem. Int. Ed.* **2011**, *50*, 4056.
[22] A. Kaeser, A. P. H. J. Schenning, *Adv. Mater.* **2010**, *22*, 2985.
[23] E. Genin, Z. Gao, J. A. Varela, J. Daniel, T. Bsaibess, I. Gosse, L. Groc, L. Cognet, M. Blanchard-Desce, *Adv. Mater.* **2014**, *26*, 2258.
[24] J. Yu, C. Wu, S. P. Sahu, L. P. Fernando, C. Szymanski, J. McNeill, *J. Am. Chem. Soc.* **2009**, *131*, 18410.
[25] J. Pecher, S. Mecking, *Chem. Rev.* **2010**, *110*, 6260.
[26] C. Wu, D. T. Chiu, *Angew. Chem. Int. Ed.* **2013**, *52*, 3086.
[27] H. Wang, P. Zhang, Y. Hong, B. Zhao, P. Yi, J. Chen, *Polym. Chem.* **2017**, *8*, 5795.
[28] K. Li, B. Liu, *Chem. Soc. Rev.* **2014**, *43*, 6570.
[29] X. Gu, R. T. K. Kwok, J. W. Y. Lam, B. Z. Tang, *Biomaterials* **2017**, *146*, 115.
[30] A. Reisch, A. S. Klymchenko, *Small* **2016**, *12*, 1968.
[31] M. P. Robin, R. K. O'Reilly, *Polym. Int.* **2015**, *64*, 174.
[32] A. Reisch, P. Didier, L. Richert, S. Oncul, Y. Arntz, Y. Mély, A. S. Klymchenko, *Nat. Commun.* **2014**, *5*.
[33] A. Reisch, K. Trofymchuk, A. Runser, G. Fleith, M. Rawiso, A. S. Klymchenko, *ACS Appl. Mater. Interfaces* **2017**, *9*, 43030.
[34] K. Trofymchuk, A. Reisch, P. Didier, F. Fras, P. Gilliot, Y. Mely, A. S. Klymchenko, *Nat. Photonics* **2017**, *11*, 657.
[35] B. Andreiuk, A. Reisch, M. Lindecker, G. Follain, N. Peyriéras, J. G. Goetz, A. S. Klymchenko, *Small* **2017**, *13*, 1701582.
[36] J. Chen, W. Zhong, Y. Tang, Z. Wu, Y. Li, P. Yi, J. Jiang, *Macromolecules* **2015**, *48*, 3500.
[37] J. S. Suk, Q. Xu, N. Kim, J. Hanes, L. M. Ensign, *Adv. Drug Deliv. Rev.* **2016**, *99, Part A*, 28.
[38] Z. G. Estephan, P. S. Schlenoff, J. B. Schlenoff, *Langmuir* **2011**, *27*, 6794.
[39] K. Luby-Phelps, *Int. Rev. Cytol.* **2000**, *192*, 189.
[40] K. Luby-Phelps, *Mol. Biol. Cell* **2013**, *24*, 2593.
[41] K. Norregaard, R. Metzler, C. M. Ritter, K. Berg-Sørensen, L. B. Oddershede, *Chem. Rev.* **2017**, *117*, 4342.
[42] F. Höfling, T. Franosch, *Rep. Prog. Phys.* **2013**, *76*, 046602.
[43] D. Wirtz, *Annu. Rev. Biophys.* **2009**, *38*, 301.
[44] J. A. Dix, A. S. Verkman, *Annu. Rev. Biophys.* **2008**, *37*, 247.
[45] H. S. Choi, W. Liu, F. Liu, K. Nasr, P. Misra, M. G. Bawendi, J. V. Frangioni, *Nat. Nanotechnol.* **2010**, *5*, 42.
[46] H. Cabral, Y. Matsumoto, K. Mizuno, Q. Chen, M. Murakami, M. Kimura, Y. Terada, M. R. Kano, K. Miyazono, M. Uesaka, N. Nishiyama, K. Kataoka, *Nat. Nanotechnol.* **2011**, *6*, 815.
[47] R. Ferrari, M. Lupi, F. Falcetta, P. Bigini, K. Paolella, F. Fiordaliso, C. Bisighini, M. Salmona, M. D'Incalci, M. Morbidelli, D. Moscatelli, P. Ubezio, *Nanotechnology* **2014**, *25*, 045102.
[48] L. Shang, K. Nienhaus, G. U. Nienhaus, *J. Nanobiotechnology* **2014**, *12*, 5.
[49] K. Luby-Phelps, D. L. Taylor, F. Lanni, *J. Cell Biol.* **1986**, *102*, 2015.
[50] E. Dauty, A. S. Verkman, *J. Biol. Chem.* **2005**, *280*, 7823.
[51] T. Kalwarczyk, N. Ziębacz, A. Bielejewska, E. Zaboklicka, K. Koynov, J. Szymański, A. Wilk, A. Patkowski, J. Gapiński, H.-J. Butt, R. Hołyst, *Nano Lett.* **2011**, *11*, 2157.
[52] L. H. Reddy, J. L. Arias, J. Nicolas, P. Couvreur, *Chem. Rev.* **2012**, *112*, 5818.
[53] F. Tang, L. Li, D. Chen, *Adv. Mater.* **2012**, *24*, 1504.

[54] F. Danhier, E. Ansorena, J. M. Silva, R. Coco, A. Le Breton, V. Preat, *J. Controlled Release* **2012**, *161*, 505.
[55] M. J. Saxton, *J. Phys. Chem. B* **2014**, *118*, 12805.
[56] K. Landfester, *Angew. Chem. Int. Ed.* **2009**, *48*, 4488.
[57] F. Candau, M. Pabon, J.-Y. Anquetil, *Colloids Surf. Physicochem. Eng. Asp.* **1999**, *153*, 47.
[58] F. Gu, L. Zhang, B. A. Teply, N. Mann, A. Wang, A. F. Radovic-Moreno, R. Langer, O. C. Farokhzad, *Proc. Natl. Acad. Sci.* **2008**, *105*, 2586.
[59] G. Riess, *Prog. Polym. Sci.* **2003**, *28*, 1107.
[60] E. Lepeltier, C. Bourgaux, P. Couvreur, *Adv. Drug Deliv. Rev.* **2014**, *71*, 86.
[61] S. Schubert, J. T. Delaney, U. S. Schubert, *Soft Matter* **2011**, *7*, 1581.
[62] A. Reisch, A. Runser, Y. Arntz, Y. Mély, A. S. Klymchenko, *ACS Nano* **2015**, *9*, 5104.
[63] F. Lince, D. L. Marchisio, A. A. Barresi, *J. Colloid Interface Sci.* **2008**, *322*, 505.
[64] W. S. Saad, R. K. Prud'homme, *Nano Today* **2016**, *11*, 212.
[65] M. Beck-Broichsitter, J. Nicolas, P. Couvreur, *Nanoscale* **2015**, *7*, 9215.
[66] M. Li, M. Jiang, L. Zhu, C. Wu, *Macromolecules* **1997**, *30*, 2201.
[67] D. Horn, J. Rieger, *Angew. Chem. Int. Ed.* **2001**, *40*, 4330.
[68] B. Andreiuk, A. Reisch, V. G. Pivovarenko, A. S. Klymchenko, *Mater. Chem. Front.* **2017**, *1*, 2309.
[69] I. Shulov, S. Oncul, A. Reisch, Y. Arntz, M. Collot, Y. Mely, A. S. Klymchenko, *Nanoscale* **2015**, *7*, 18198.
[70] M. Tokunaga, N. Imamoto, K. Sakata-Sogawa, *Nat. Methods* **2008**, *5*, 159.
[71] N. Ruthardt, D. C. Lamb, C. Bräuchle, *Mol. Ther.* **2011**, *19*, 1199.
[72] C. D. Rienzo, E. Gratton, F. Beltram, F. Cardarelli, *Proc. Natl. Acad. Sci.* **2013**, *110*, 12307.
[73] H. Li, S.-X. Dou, Y.-R. Liu, W. Li, P. Xie, W.-C. Wang, P.-Y. Wang, *J. Am. Chem. Soc.* **2015**, *137*, 436.
[74] K. Susumu, E. Oh, J. B. Delehanty, F. Pinaud, K. B. Gemmill, S. Walper, J. Breger, M. J. Schroeder, M. H. Stewart, V. Jain, C. M. Whitaker, A. L. Huston, I. L. Medintz, *Chem. Mater.* **2014**, *26*, 5327.
[75] E. Derivery, E. Bartolami, S. Matile, M. Gonzalez-Gaitan, *J. Am. Chem. Soc.* **2017**, *139*, 10172.
[76] T. Kalwarczyk, K. Sozanski, A. Ochab-Marcinek, J. Szymanski, M. Tabaka, S. Hou, R. Holyst, *Adv. Colloid Interface Sci.* **2015**, *223*, 55.
[77] D. W. Provance, A. McDowall, M. Marko, K. Luby-Phelps, *J. Cell Sci.* **1993**, *106 (Pt 2)*, 565.
[78] C. Kronlage, M. Schäfer-Herte, D. Böning, H. Oberleithner, J. Fels, *Biophys. J.* **2015**, *109*, 687.
[79] M. E. Grady, E. Parrish, M. A. Caporizzo, S. C. Seeger, R. J. Composto, D. M. Eckmann, *Soft Matter* **2017**, *13*, 1873.
[80] L. W. Janson, K. Ragsdale, K. Luby-Phelps, *Biophys. J.* **1996**, *71*, 1228.
[81] B. R. Parry, I. V. Surovtsev, M. T. Cabeen, C. S. O'Hern, E. R. Dufresne, C. Jacobs-Wagner, *Cell* **2014**, *156*, 183.
[82] C. Würth, D. Geißler, T. Behnke, M. Kaiser, U. Resch-Genger, *Anal. Bioanal. Chem.* **2014**, *407*, 59.
[83] P. Müller, P. Schwille, T. Weidemann, *Bioinformatics* **2014**, *30*, 2532.
[84] I. F. Sbalzarini, P. Koumoutsakos, *J. Struct. Biol.* **2005**, *151*, 182.

What is the ideal size for nanoparticles for intracellular applications? Here, a series of dye-loaded polymer nanoparticles with sizes from 50 down to 7 nm is synthesized and microinjected into living cells. Single-particle tracking of these particles suggests that only NPs smaller than a critical size of 23 nm exhibit free diffusion and spreading in the cytosol.

Keyword: nanoparticles in the cytosol

A. Reisch,* D. Heimburger, P. Ernst, A. Runser, P. Didier, D. Dujardin, and A. S. Klymchenko*

Protein-sized Dye-loaded Polymer Nanoparticles for Free Particle Diffusion in Cytosol